Scaling of sensitivity and efficiency in planar microresonators for electron spin resonance

R. Narkowicz,[1,2] D. Suter,[1] and I. Niemeyer[1]
[1]*Department of Physics, Technical University of Dortmund, D-44221 Dortmund, Germany*
[2]*Semiconductor Physics Institute, LT-01108 Vilnius, Lithuania*

(Received 8 March 2008; accepted 6 July 2008; published online 13 August 2008)

Electron spin resonance (ESR) of volume-limited samples or nanostructured materials can be made significantly more efficient by using microresonators whose size matches that of the structures under investigation. We describe a series of planar microresonators that show large improvements over conventional ESR resonators in terms of microwave conversion efficiency (microwave field strength for a given input power) and sensitivity (minimum number of detectable spins). We explore the dependence of these parameters on the size of the resonator and find that both scale almost linearly with the inverse of the resonator size. Scaling down the loops of the planar microresonators from 500 down to 20 μm improves the microwave efficiency and the sensitivity of these structures by more than an order of magnitude and reduces the microwave power requirements by more than two orders of magnitude. © *2008 American Institute of Physics.* [DOI: 10.1063/1.2964926]

I. INTRODUCTION

Electron spin resonance (ESR) experiments are based on the interaction between magnetic dipoles (spins) in the sample and applied microwave magnetic fields. Since this interaction is relatively weak, it is usually necessary to increase this coupling with the help of a resonant structure, the ESR resonator. There are generally two ways to optimize the resonator performance at a given frequency—to increase its quality factor or the filling factor. Which of the two methods is optimal depends on the sample and the type of the experiment. For relatively large samples, the best results may be achieved using the classical cavities with optimized quality factor, whereas for small samples increasing the filling factor by adjusting the resonator to the sample size provides better results. Small nonresonant microcoils, just surrounding the sample, improve the conversion efficiency by concentrating the microwave field in the sample area.[1,2] The conversion efficiency further improves if the microcoils are tuned and matched to the impedance of the feed line.[3–6] At higher frequencies (*Q* to *W* band), loop-gap resonators with a loop size of a few hundred micrometers are better suited.[7–9] The above mentioned noncavity structures have been found useful in single spin experiments if they are combined with alternative detection techniques, such as magnetic resonance force microscopy,[10] optical detection,[11] or electrical detection of the tunneling current.[12] Unfortunately, these alternative detection schemes cannot be applied to all samples and do not represent a universal alternative to the inductive detection method. Therefore we want to explore the possibilities for increasing the sensitivity of the inductive detection by using small resonators for excitation and detection, which concentrate the microwave field in the sample region. They provide efficient conversion of microwave power into magnetic field and, conversely, an efficient conversion of magnetic flux from the precessing magnetization into a traveling electromagnetic field to be detected by the spectrometer.

So far, the work on noncavity microresonators has concentrated on demonstrating the possibility of using subwavelength resonators for specific applications. Here, we are specifically interested in exploring the efficiency of these microresonators as a function of their size: how does the conversion of microwave energy into magnetic field strength depend on the size of the resonator, and how does the detection sensitivity scale with the same parameter? Peck *et al.*[13] analyzed this issue for the case of solenoidal NMR microcoils with coil diameters D_i down to 50 μm. They theoretically predicted and experimentally verified that the signal to noise ratio should scale as $1/D_i$ as long as the wire diameter exceeds the skin depth of the radio frequency field in the metal used (Cu). Similar behavior should apply for the planar NMR microcoils, as well as the microslot probes based on the microstripline design.[14] The linear sensitivity scaling with the inverse coil diameter was theoretically extrapolated to the ESR experiments at frequencies up to that of the *X* band.[4] Here we investigate this dependence experimentally for resonators just above the *X* band (14 GHz).

In this paper, we describe the design, construction, and testing of planar microresonators (PMRs) for ESR over the size range of 500 down to 20 μm. This type of microresonator is well suited for scaling to very small sizes since it can be constructed by lithographic techniques. Each resonator consists of an inductive loop and tuning elements that adjust the overall impedance to match the impedance of the transmission line (50 Ω). Experimental verification over the range of the scaled down designs demonstrated that conversion efficiency and sensitivity scale with the coil diameter approximately as $D_i^{-\alpha}$, with $\alpha \sim 0.8-1$.

II. DESIGN OF PMRs

Our PMR structures consist of a planar loop, whose diameter is much smaller than the operation wavelength, and

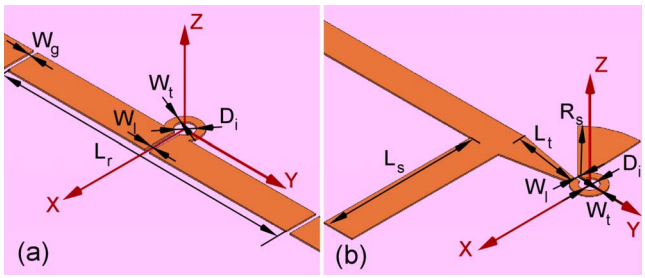

FIG. 1. (Color online) Basic layout of the two PMRs. For both layouts, D_i stands for the loop diameter, W_t for the trace width, and W_l is the width of the gap in the loop. Specific tuning and matching parameters are (a) resonator length L_r and gap width W_g, (b) radial stub radius R_s, rectangular stub length L_s, and taper length L_t. Both layouts were realized on a 12 $\times$12 mm^2 TMM10i substrate with thickness D_s=380 μm. The ground plane of both resonators was fully metallized.

distributed tuning and matching elements. The structure is connected to a 50 Ω coaxial line via a microstrip line and a subminiature version A (SMA) coaxial-to-microstrip connector.[15] To minimize reflection losses, the structure is tuned and matched to the 50 Ω impedance of the coaxial and microstrip line. We explored two slightly different designs, which are shown schematically in Fig. 1. In the Ω-shaped design shown in Fig. 1(a), tuning is achieved by adjusting the length of the microstrip line section L_r and matching via the width W_g of the gap at its ends. In the second design [Fig. 1(b)], the radial stub serves as a tuning element and the rectangular stub as the matching element. In the following we call this design an R-shaped PMR. The R-shaped PMR is used in reflection geometry; the Ω-shaped design can be used in reflection or transmission. In the reflection configuration, the second port is attached to a SMA connector and can either be connected to a 50 Ω SMA resistor or left open. Simulation shows that with the 50 Ω resistor, the resonator exhibits behavior similar to that found in the transmission experiment and is somewhat undercoupled. Leaving the second port open shifts the resonance frequency down by up to 100 MHz. The resonator is then slightly overcoupled, and its Q factor increases by 30% compared to the transmission configuration. Both designs were implemented and tested in an earlier work[5] for loop diameters of 200 and 500 μm.

We started the design of smaller PMRs by scaling down the dimensions of the loop, which is the structure that concentrates the magnetic field and couples to the sample inside it. To determine the optimal trace width of the loop structure, we used the ratio of the emf induced in the loop by the precessing magnetization to the noise voltage generated by its active resistance r_i as the main criterion. The emf is proportional to the magnetic field B_{1u}, produced by a unit current in the loop, while the noise is proportional to $\sqrt{r_i}$.[16] The microwave field strength B_{1u} in the loop was approximated by the value of B_{1u} in the center of the loop, calculated using the quasistatic approach.[5] Maximizing the ratio $B_{1u}/\sqrt{r_i}$, we found that the optimal trace width W_t should be roughly proportional to the loop diameter D_i.

Apart from the trace width, the active resistance of the loop could also be minimized by using a thicker metallization layer, but technological constraints limited the aspect ratio of the loop height T_m to its width to about 1. The skin depth at the frequency of operation (14 GHz) is 0.55 μm and remains small compared to other dimensions for all of the tested layouts. Accordingly, only the surface of the structure contributes significantly to the conductance. Using these criteria, we selected the relevant parameters for six different resonators whose loop diameter varied between 10 and 500 μm (see Table I). For each resonator, we also calculated the inductance according to the loop inductance approximation from Ref. 17. The inductance decreases slightly less than the linear dimensions of the loop. In order to keep the loop tuned to the fixed operation frequency of the spectrometer (14 GHz in our case) and matched to the 50 Ω coaxial input of the preamplifier, an adequate modification of the tuning and matching elements was required.

TABLE I. Loop dimensions and inductances.

D_i (μm)	W_l (μm)	W_t (μm)	T_m (μm)	L (nH)
500	200	220	35	0.81
200	60	80	17.5	0.33
100	30	30	17.5	0.17
50	15	15	15	0.084
20	6	6	6	0.035
10	3	3	3	0.023

The dimensions of the tuning and matching elements were determined numerically. The multiparameter optimization required for this purpose was performed using the commercial microwave simulator HFSS V.10 (Ansoft). The procedure included simultaneous optimization of different design parameters. In the case of the Ω-shaped resonator, we optimized the microstrip line length L_r and the gap width W_g, and in the R-shaped design the radial stub radius R_s, the length of the taper L_t between the feeding microstrip line and the loop, and the rectangular stub length L_s. The model that we used included not only the actual resonator but also the coaxial connectors and the chip holder. As the quality criterion for the optimization, we chose minimal reflection at the resonance frequency. Attempts to directly use the magnetic field strength in the coil as the optimization criterion led to relatively poor tuning and matching of the PMR; so, the resulting designs were discarded.

The simulation model of HFSS is based on a finite element method. The program solves Maxwell's equations on a three-dimensional adaptive tetragonal mesh. The mesh, together with an appropriate set of boundary conditions, represents the geometric structure of the PMR. Additional (higher resolution) meshing constraints were applied in those areas where we expected large electric field gradients, as well as in the inner part of the loop, in order to obtain smooth magnetic field profiles in this area. This reduced the total number of the tetragons compared to the automated meshing algorithm and led to faster optimization. The final mesh size for different layouts varied from 40 000 up to 150 000 tetragons, and the simulation took from 30 min up to 5 h of CPU time on a standard PC.

The conduction losses in the metallic part of the PMR were taken into account by boundaries with finite conductivity, without calculating the field distribution inside the metal.

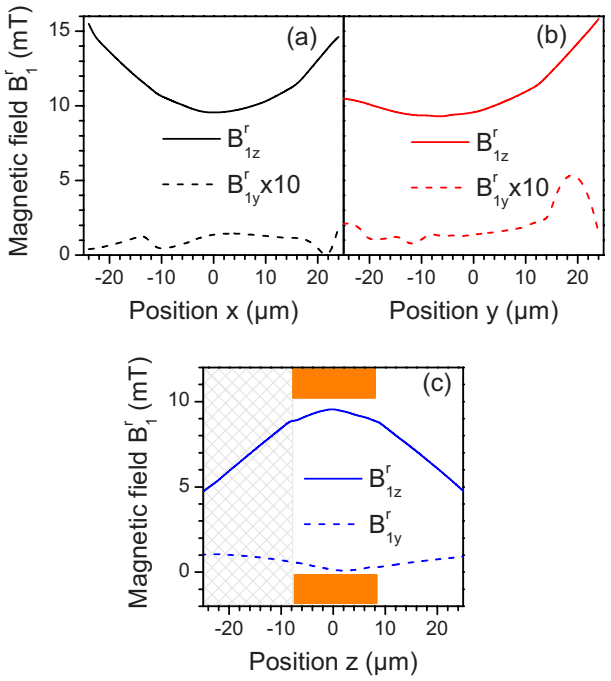

FIG. 2. (Color online) Simulated distribution of the components of the microwave magnetic field $B(t)=2B_1^r \cos \omega t$ perpendicular to the static field $\mathbf{B_0} \| x$ in the 50 μm PMR loop: (a) and (b) as a function of x and y, i.e., in the loop plane; (c) perpendicular to the loop plane. The hatched rectangle in panel (c) indicates the substrate; the full rectangles show the loop rim (Cu). The coordinate system is the same as in Fig. 1. The magnetic field values correspond to an input power $P_{\mu w}=1$ W.

For the largest loop diameter of 500 μm, despite the open structure of the PMR, no serious resonance broadening (indicating increased radiation losses) was found, as long as the bottom of the PMR substrate was fully metallized, forming the ground plane. This was checked by simulating the PMR within the absorbing (called "radiation") and reflecting ("finite conductivity") boundaries. No significant change in the PMR resonance was observed. Removing the shield under the loop not only tuned the PMR away from the expected resonance but also strongly broadened the observed resonance, indicating increased radiation losses.

From this simulation, we obtained the dimensions of the PMR, the frequency dependence of the reflection coefficient, and the field distribution at the operation frequency. The dimensions of the PMR and the simulated frequency dependence of the reflection coefficient will be discussed in detail in Sec. III, where the latter will be compared to the network analyzer measurements. Here, we look in more detail at the field distribution within the loop.

For the excitation of the spins, we have to consider the microwave field components perpendicular to the static field, which is oriented along the x axis of the resonators. The main contribution therefore stems from the z component, perpendicular to the plane of the loop, with only a minor contribution from the in-plane component along the y direction. As shown in Fig. 2(a), the z component of the microwave field has approximately cylindrical symmetry, except for the gap in the loop, where the field amplitude is close to its minimal value in the loop center [Fig. 2(b)]. In the direction perpendicular to the loop plane, the microwave magnetic field remains approximately constant within the loop but quickly decays outside [Fig. 2(c)]. Figure 2 shows the distribution for the case of the 50 μm resonator; for the other resonators, the field distribution in the area of the loop scales with the loop diameter.

For some applications, it is important to keep the electric field component in the sample area small; this is particularly important for samples with finite conductivity, such as semiconductors or ionic liquids, where the electric field component can cause undesirable sample heating. In addition, samples with a high dielectric constant cause a detuning of the resonator proportional to the electric field strength in the sample area. The simulation shows that in both PMR types the electric field is concentrated on the outer edges of the tuning elements (Fig. 3). In the sample region, the electric field is less than 10% of the maximum value. The electric field in the Ω-shaped PMR is even smaller, because the null of the E-field occurs at the loop position. The strength of the electric field does not change significantly with the size of the loop, and its distribution remains roughly constant.

In the experiment, the influence of the electric field at the sample position in the PMR is evidenced qualitatively by the shift of the resonance with sample loading. We measured shifts on the order of a few megahertz when a small 2,2-diphenyl-1-picrylhydrasil (DPPH) crystal was placed in the loop center, and up to 130 MHz when the loop was fully loaded with a powder sample.

As a criterion for the efficiency of the resonators, we use

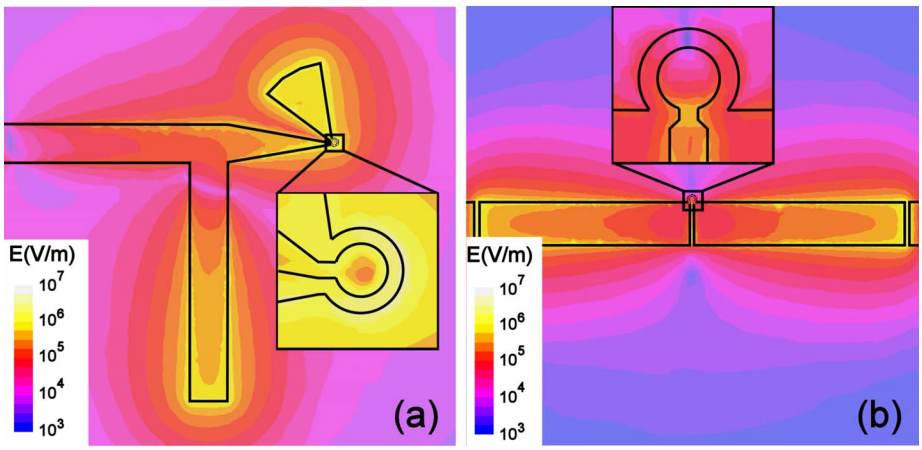

FIG. 3. (Color online) Simulated electric field distribution in both microresonators: (a) Ω-shaped PMR and (b) R-shaped PMR. The presented E-field distributions are shown for the PMRs with 50 μm loop diameter, but they are typical for other sizes.

the microwave conversion factor $\Lambda = B_1^r / \sqrt{P_{\mu w}}$,[18] which quantifies the conversion of the microwave power $P_{\mu w}$ into magnetic field strength $B(t) = 2B_1^r \cos \omega t$, and is proportional to the unitary magnetic field. Since the magnetic field varies with position, we use its value at the center of the loop to compare different resonators. For the largest resonator with a 500 μm diameter loop, the microwave efficiency is 1 $mT/W^{1/2}$, i.e., more than an order of magnitude higher than that of the TE_{102} microwave cavity.[19] For smaller resonators, the efficiency improves almost linearly with the inverse size of the loop (see Sec. IV A).

III. MANUFACTURING AND VERIFICATION

The resonators were manufactured on substrates with well-controlled thickness (640 and 380 μm), dielectric constant $\varepsilon_r = 9.8$, and losses tan $\delta = 0.002$ (TMM10i, Rogers). The optimized designs obtained from the simulation were written to a photomask and by optical lithography transferred to high aspect ratio photoresists covering the TMM10i substrates.

The Ω-shaped PMRs with 500 μm loop diameter were etched on 0.64 mm thick substrates with 17.5 μm double-sided copper cladding. With these substrates, the etching process allowed minimal feature sizes down to 100 μm. This resolution was not sufficient for PMR layouts with a loop diameter of 200 μm and smaller. To achieve higher resolution, we used a 0.38 mm thick TMM10i substrate without metallization on the top side and created a patterned metallization layer.[20] To improve adhesion, we first sputtered a thin Ti layer and on top of it the 300 nm copper seed layer. We covered this layer with a high aspect ratio photoresist, patterned it in a photolithographic process, and by electroplating, deposited in the grooves up to 20 μm of copper. Finally, we stripped the photoresist and removed the seed layer from the areas where the photoresist had covered it by etching. With this process, the minimum feature size was about 6 μm.

The finished PMRs were cut and mounted in a holder with SMA connectors for testing with the network analyzer. The resonance frequencies f_0 and the quality factors Q_l were determined from the power reflection coefficient data (Table II). For better comparison with the HFSS simulation results, quality factors $Q_{-3\ dB}$, calculated from the half-power resonance bandwidth, were extrapolated to the case of critical coupling. The coupling coefficient β was obtained from the Smith chart of the tuning curve and used to determine an unloaded quality factor $Q = (1+\beta) Q_{-3\ dB}$. The latter allowed the loaded quality factor $Q_l = Q/2$ to be calculated.

Inspection of the simulated PMR dimensions indicates that scaling down the loop in the Ω-shaped layout requires longer microstrip lines to tune it to the operation frequency. For small loop size, the overall length L_r approaches a constant length, slightly below $\lambda/2 = 4.2$ mm of the microstrip resonator. For the R-shaped layout, the dimensions (apart from the loop) remain roughly constant.

For every layout listed in Table II, we manufactured two resonators. Their measured frequencies agreed with the simulated resonance frequencies within ~1%. The quality factors of the PMRs were more sensitive to the variations in the dimensions of tuning and matching elements. The Q_l values for R-shaped PMRs vary on average within 11% from the predicted values, while the Q_l's for Ω-shaped PMRs are on average 50% smaller than the simulated values. The main sources for the manufacturing tolerances are insufficient control over the electrodeposition process and imperfections in the lithography. For example, the sidewalls of the metal layer were not vertical, which may be the result of a slight underetching of the photoresist. Another possible source of systematic deviation may be the interface roughness, which was not taken into account in the modeling. In the pores of the substrate, some part of the titanium adhesion layer might also remain and thereby contribute to the performance degradation. The quality factor of the R-shaped resonator was consistently higher than that of the Ω-shaped PMRs, with the biggest differences in the experimental values for the smallest resonators.

TABLE II. Microwave parameters of the PMRs. f_{0th} and Q_{lth} are the resonance frequency and quality factor obtained from the simulated power reflection curves; f_{0e} and Q_{le} were measured with a calibrated Wiltron 360B network analyzer on the empty PMRs. The geometrical parameters of the PMRs are defined in Fig. 1. Both experimental and theoretical quality factors were extrapolated to the case of a critical coupling.

R-shaped PMRs							
D_i (μm)	R_s (mm)	L_t (mm)	L_s (mm)	f_{0th} (GHz)	Q_{lth}	f_{0e} (GHz)	Q_{le}
200	0.80	0.73	2.22	14	62	13.95	46
100	0.70	0.90	2.59	13.97	57	13.92	59
50	0.74	0.96	2.59	13.99	54	13.92	52
20	1.13	0.64	2.15	14	45	13.88	55
Ω -shaped PMRs							
D_i (μm)	L_r (mm)	W_g (μm)		f_{0th} (GHz)	Q_{lth}	f_{0e} (GHz)	Q_{le}
500	2.28	200		13.98	41	13.81	27
200	3.35	50		13.97	38	13.72	27
100	3.48	39		14.02	32	14.05	16
50	3.56	49		14.1	32	13.89	15
20	3.62	50		14	35	13.85	14

As we already mentioned, the sample, whose size was roughly half of the loop diameter had only a minor effect on the resonance frequency and quality factor of the PMR (Fig. 4). Bigger samples shifted the resonance down by up to 130 MHz.

If the resonance of a PMR differs from the design values or is not deep enough, it can be tuned and matched in the final device by placing pieces of dielectric material over the areas of strong electric field. Suitable places include the edges of the stub in the case of the R-shaped PMR and the gaps in the microstrip line in the case of the Ω-shaped PMR. In this way we have improved matching of the R-type PMR with 100 μm loop from −9 to −22 dB. This resulted also in a frequency downshift of 400 MHz. Because of the limited bandwidth of our microwave source, we did not apply the additional matching for the PMRs where matching was initially acceptable but not perfect (Fig. 4).

The TMM-type substrates that we used were manufactured for space flight conditions. Accordingly, they provide

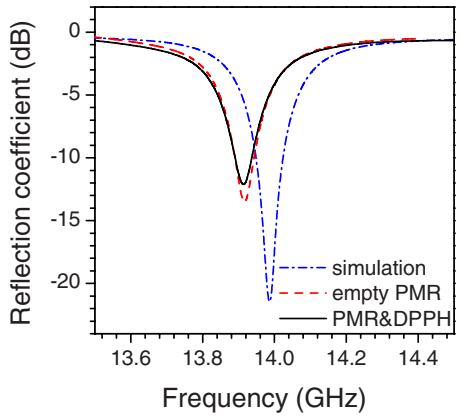

FIG. 4. (Color online) Experimental and simulated tuning curves of the R-shaped PMR with a 50 μm diameter loop. The curve marked "PMR&DPPH" was measured for the resonator loaded with sample.

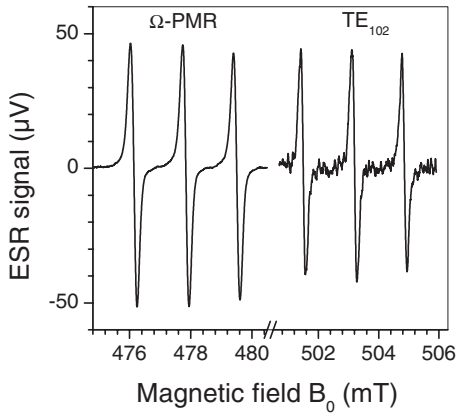

FIG. 6. ESR spectrum of TEMPOL dissolved in water (3 mM/l). For the PMR the microwave power was 69 μW, the microwave frequency was 13.414 GHz, the sweep rate was 50 μT/s, the field modulation frequency was 100 kHz, and the modulation amplitude was 100 μT. For the TE_{102} cavity the microwave power was 2.5 mW, the microwave frequency was 14.126 GHz, the sweep rate was 40 μT/s, the field modulation frequency was 2 kHz, and the modulation amplitude was 140 μT. Both spectra were measured with the lock-in time constant 0.3 s in a single sweep, without averaging.

excellent thermal stability of the dielectric constant ε_r and geometric parameters. The manufacturer provides thermal expansion and ε_r thermal coefficients down to −55 °C. Testing the PMRs at low temperatures, we measured the reflection coefficient of the empty Ω-shaped PMR with D_i=500 μm. Figure 5 shows the measured tuning curves. Over the temperature range from room temperature down to liquid nitrogen temperature, we used a Wiltron 360B vector network analyzer. The data at 2 K were collected from the same resonator in liquid helium with a scalar network analyzer (Anritsu 54147A).

From 300 down to 79 K, the resonance frequency and the quality factor remained quite stable. Maximal variation of the resonance frequency did not exceed 54 MHz, while the quality factor varied by less than 10% of its room temperature value. In liquid He (T=2 K), the resonance was downshifted by about 220 MHz from its room temperature position. The resonator was loaded with sample for the 2 K measurement, while it was empty in the other measurements. Judging from room temperature measurements, we estimate that ~40 MHz of the frequency shift is due to the loading by the sample, while the rest is mostly due to the dielectric constant of liquid helium.

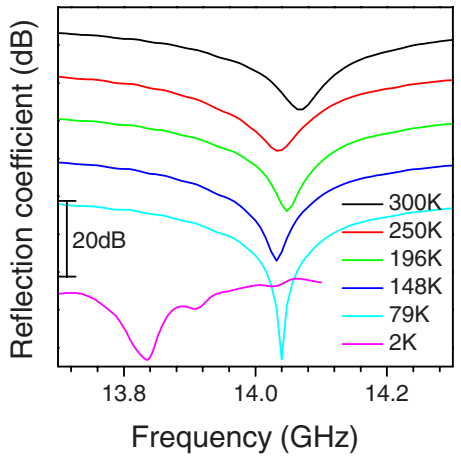

FIG. 5. (Color online) Temperature dependence of the tuning curve. The distortions on the curve measured at 2 K are due to interference in the long coaxial lines connecting the PMR chip to the network analyzer. The scale bar length corresponds to 20 dB. The individual curves are shifted vertically to avoid overlap.

IV. ESR EXPERIMENTS

ESR experiments were performed using a 14 GHz home-built spectrometer. Details on the spectrometer can be found in the Ref. 5.

For a first test experiment, we used a sample consisting of 4-hydroxy-2,2,6,6-tetramethylpiperidine-1-oxyl (TEMPOL), dissolved in water. The sample was held in a 400 μm outside diameter (300 μm inside diameter) quartz capillary tube, which was inserted into the via hole drilled in the loop of the 500 μm diameter Ω-shaped PMR. The measured spectrum for this nitroxide radical (Fig. 6) was similar to the spectra obtained at X band.[21] For comparison, we measured the same 3 mM/l concentration sample in the TE_{102} cavity. Both spectra have the same signal height in spite of the 43 times larger sample volume in the cavity. The sample dimensions in the cavity are defined by the inside diameter of capillary (300 μm) and the width of the cavity (15 mm). For the PMR, we calculated effective sample dimensions of 300 μm (inside diameter of the capillary) in the resonator plane and 350 μm perpendicular to it by integrating the microwave field from the simulation.

Figure 7 shows the measured amplitudes of the absorption and dispersion signal versus microwave input power P_{in} for the 500 μm Ω-shaped resonator. The absorption signal has a distinct maximum at P_{in}=90 μW, indicating that the sample saturates, while the dispersion signal does not reach a maximum up to 400 μW.

For testing the smaller PMRs, we used small grains of DPPH (Fig. 8). The crystal diameters were about half of the resonator diameter, and efforts were made to place them close to the center of the loop. The samples were fixed inside the resonators using silicone sealant.

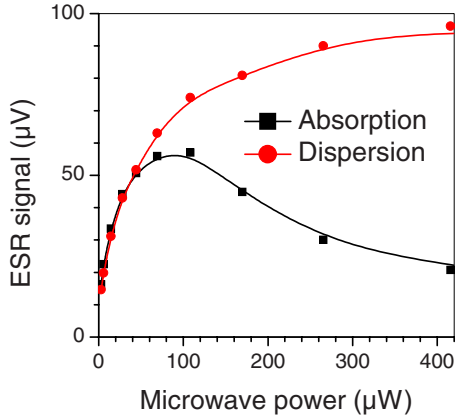

FIG. 7. (Color online) Power dependence of the ESR signal from the 3 mM/l TEMPOL sample, measured in the PMR with the field modulation amplitude of 110 μT. The other parameters are the same as mentioned in the caption of Fig. 6.

A. B_1 Field measurements by nutation

We determined the microwave efficiency factor Λ of the PMRs by measuring the strength of the microwave field in the resonator by spin nutation experiments. In these experiments, we applied a microwave excitation pulse of variable duration and then recorded the free induction decay (FID) signals. Figure 9(a) shows the amplitude of the resulting nutation signals as a function of the pulse duration for different microwave powers.

In Fig. 9, we also compare these experimental results to the theoretically expected behavior. For this calculation, we used the spatial distribution of the field strength obtained from the simulation of the PMR. Due to the reciprocity principle, different parts of the sample contribute differently to the overall signal.[22] We take this into account by a suitably weighted average,

$$S \propto \exp(-\tau/T_2) \int_{V_s} B^r_{1yz}(\mathbf{r}) \sin[\gamma B^r_{1yz}(\mathbf{r})\tau] dV. \quad (1)$$

Here, S is the signal, $B^r_{1yz}(\mathbf{r})$ is the magnetic field component perpendicular to the external magnetic field, T_2=62 ns (Ref. 23) is the transverse relaxation time for DPPH, γ is the gyromagnetic ratio for DPPH, and τ is the pulse duration. The resulting average signal can be approximated by an exponentially damped sine function

$$S = S_0 \exp(-\tau/T_m)\sin(\gamma B^r_1 \tau). \quad (2)$$

Here, B^r_1 stands for the average value of the transverse magnetic field component and T_m is the decay time. This overall decay includes the effect from the inhomogeneous microwave field and the spin relaxation.

The measured nutation curves were fitted with the damped sine function [Eq. (2)] to determine the amplitude B^r_1 of the microwave field and the microwave efficiency Λ. We found that the microwave efficiency scales linearly with the inverse loop diameter of the PMR, as in the simulation, but the values were about 50% smaller than the theoretical ones (Fig. 10). In spite of the considerably smaller quality factors, the microwave efficiency of the 50 μm Ω-shaped PMR is comparable to that of the R-shaped design at the same loop size.

The most probable explanation of the discrepancy between the experimental and calculated Λ values appears to be additional losses that were not taken into account in the simulation. Both the dielectric loss in the substrate material

FIG. 8. (Color online) Photograph of the 50 μm R-shaped PMR with a DPPH grain in the center of the loop.

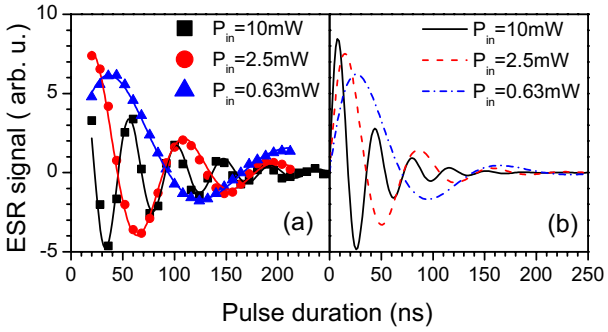

FIG. 9. (Color online) Dependence of FID signal amplitude on the excitation pulse length and input power measured in the R-shaped PMR with loop diameter of 50 μm: (a) measurements, (b) simulation. The simulated signal decay includes the effects of the microwave field inhomogeneity and spin relaxation.

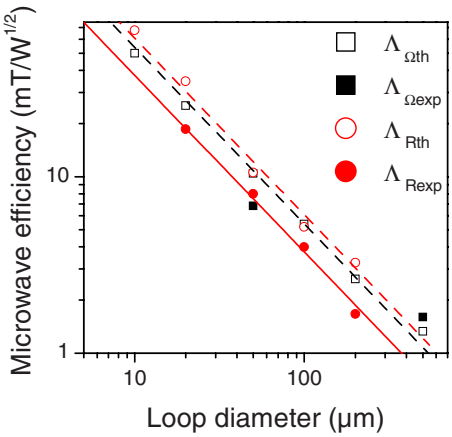

FIG. 10. (Color online) Microwave efficiencies simulated and measured in the nutation experiment. For the Ω-shaped PMRs, the open squares stand for the calculated ($\Lambda_{\Omega th}$) and the full squares for the measured ($\Lambda_{\Omega\,exp}$) values. Theoretical (Λ_{Rth}) and experimental ($\Lambda_{R\,exp}$) values for the R-shaped PMR are depicted by the open and closed circles, respectively. The dashed lines represent a linear fit to the simulated data, and the solid line the fit to the experimental data.

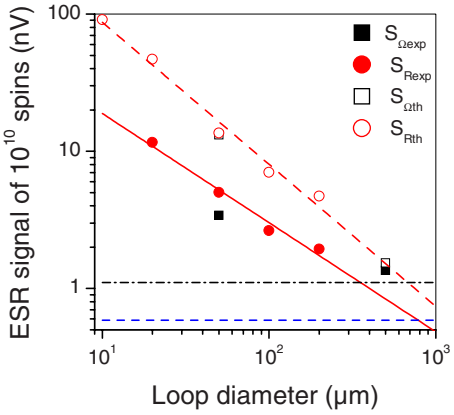

FIG. 11. (Color online) cw ESR signal amplitude at the receiver input, normalized to 10^{10} spins, as a function of the loop diameter. For the Ω-shaped PMRs, the open squares stand for the calculated ($S_{\Omega th}$) and the full squares for the measured ($S_{\Omega\,exp}$) signal values. For the R-shaped PMRs, open circles correspond to the theoretical (S_{Rth}) and the full circles to the experimental ($S_{R\,exp}$) signal values. The dashed line represents a linear fit to the simulated data, while the solid line is a power function fitted to the experimental data [signal (nV)$=118/D_i^{0.8}$ (μm)]. The horizontal dash-dotted line corresponds to the experimental noise level, and the dashed line marks the (theoretical) thermal noise level of a 50 Ω resistor at room temperature, for a bandwidth of 0.417 Hz.

and the conduction loss in the copper metallization were included in the simulation. The lower efficiency (corresponding to larger losses) measured in the nutation experiment are probably related to the same issues discussed for the quality factor (see Sec. III).

B. PMR sensitivity (cw measurements)

Along with the microwave efficiency, the detection sensitivity of the PMR should also increase as its size gets smaller. We tested this by quantitative measurements of cw ESR spectra. For the comparison, we use the peak-to-peak signal amplitude in the derivative of the absorption spectrum, at a microwave field strength of $B_1^r=20$ μT. At this field strength, the absorption signal is on the order of 70% of its maximum value, but saturation effects are still small. For the 500 μm Ω-shaped PMR, the signal was saturated at the power level corresponding to this field strength; so, the data were taken at $B_1^r \approx 10$ μT.

As a measure of the sensitivity, we used the absorption signal amplitude (in volts) per spin. For the normalization, we estimated the DPPH crystal volume from the calibrated pictures made with the microscope. Using the spin density of DPPH, $n_s=2\times10^{27}$ m^{-3}, we calculated the number of spins N_s in the loop of the PMR. Figure 11 shows the measured signal at the receiver input scaled to a constant number of spins ($N_s=10^{10}$). This is compared to the experimental and theoretical noise levels at the input of the receiver. For these measurements, the time constant of the lock-in amplifier was 0.3 s.

The emf generated in the loop of the PMR by the precessing magnetization was calculated using the reciprocity principle[22] and the magnetization value obtained from the Bloch equations under nonsaturation condition $[(\gamma B_1^r)^2 T_1 T_2 = 1]$:

$$\varepsilon_0 = \frac{1}{2}\gamma B_0 M_0 \sqrt{\frac{T_2}{T_1}}\frac{1}{I}\int_{V_s} B_{1yz}^r dV. \tag{3}$$

Here T_1 stands for the longitudinal relaxation time, I is the current in the loop, and M_0 is the static equilibrium magnetization. Using the HFSS field calculator, we integrated the microwave magnetic field component $B_{1yz}^r(r)$ over the sample volume and calculated the current in the loop $I=(1/\mu_0)\oint \mathbf{B}_1\cdot\mathbf{dl}$.

We finally obtained the signal at the input of the preamplifier $S_{\rm in}$, taking into account the transformation coefficient of the tuning and matching circuit, connecting the loop to the microstrip feed line:

$$S_{\rm in} = \frac{\sqrt{\beta}}{1+\beta}\sqrt{\frac{Z_0}{r_i}}\varepsilon_0. \tag{4}$$

Here Z_0 is the impedance of the transmission line (50 Ω) and r_i is the loop resistance, calculated as $r_i=2P_{\rm in}/I^2$.

To compare the simulated signal with the experimental values obtained with the field modulation technique as the derivative of the absorption signal, we use the following equation for the first derivative of the Lorentzian line:

$$\left(\frac{dS_{\rm in}}{dB}\right)_{\rm pp} = \frac{\pi\sqrt{3}}{2}2a_{1\rm pp}\frac{S_{\rm in}}{\Delta B_{\rm pp}}. \tag{5}$$

Here, $\Delta B_{\rm pp}$ is the linewidth of the absorption signal, measured as peak-to-peak distance in the derivative signal. The coefficient $a_{1\rm pp}$ depends on the modulation amplitude;[24] for our measurements, we evaluated it to be between 0.31 and 0.41.

The solid straight line in Fig. 11 corresponds to a power function. It fits the experimental data quite well for an exponent of −0.8. The scaling is thus slightly less steep than the theoretically calculated value of −1 (dashed line), similar to what we found in the scaling of the microwave efficiency. While the simulated emf ε_0/N_s scales exactly linearly with the inverse loop diameter, the value of the signal $S_{\rm in}/N_s$ has some dispersion related to the coupling coefficient β and the variations of the loop resistance r_i. The reduced scaling of the experimental curve is related to the line broadening from 2 G for the larger resonators up to 2.6 G, observed in the PMRs with 20 μm loop size. The broadening observed for the smallest PMRs is not due to overmodulation or power broadening and is most likely due to B_0 field distortion coming from the loop or the substrate material. As in the case of the microwave efficiency, the experimental signal values are consistently lower than the theoretical ones. Possible reasons for that were discussed in Sec. III. An additional experimental uncertainty is the estimated sample volume, from which we determined the number of spins in the sample.

The signal size of the Ω-shaped 500 μm resonator is quite close to the simulated value and lies above the fitting curve for the R-shaped resonators. For $D_i=50$ μm, the signal of the R-shaped PMR is about 40% larger than that from the Ω-shaped resonator. This agrees qualitatively with the expectation that the signal should scale with $Q^{1/2}$. The quality factors of these two resonators are 63 and 16, so $(Q_1/Q_2)^{1/2}\sim 2$, slightly larger than the ratio of the two sensitivities.

V. CONCLUSIONS

We have developed and tested high sensitivity planar microresonator structures for ESR experiments on small samples. These microresonators have excellent microwave efficiencies: strong microwave fields can be generated with very little microwave power and therefore low power dissipation. The reduced power dissipation is an important advantage for low temperature experiments. The small dimension and open design make them well suited for applications in nanoelectronics, spintronics, and quantum information processing. Since the structures have relatively low Q factors, their time constants are much shorter than those of conventional resonators. In addition to the ESR experiments presented here, the performance of the PMRs was also confirmed in optically detected magnetic resonance experiments with small samples.[11]

Scaling down the loops of the PMRs from 500 to 20 μm enhances the microwave efficiency and the sensitivity of these structures by more than an order of magnitude. The microwave efficiency scales linearly with the inverse loop diameter, while the sensitivity has a slightly weaker dependence. For the operation of the largest and smallest resonators tested here, the microwave power requirement dropped from 33 to 0.3 μW for $B_1=10$ μT (for cw experiments), and from 78 to 0.6 mW for pulsed operation, keeping the $\pi/2$ pulse duration constant at $t_{\pi/2}\approx 20$ ns. Using electron beam lithography, it may be possible to reduce the loop diameter further, to <1 μm. Recent developments in photonic crystals demonstrated the possibility of building 300 nm diameter planar split ring resonators, operated at terahertz frequencies.[25] The layouts presented here were designed for operation at 14 GHz, but the same tuning and matching layouts could be modified to work at other frequencies, such as X band (9.5 GHz).

If we work with such small resonators, we have to handle microscopic samples. Even with the smallest available capillaries, it becomes increasingly difficult to position the sample into the loop of the PMR. Alternative techniques, such as microcontact printing[26] might turn out to be helpful, or lithographic techniques similar to the ones used for manufacturing the resonators. The PMRs can be produced in large quantities and their parameters are quite well controlled, so their design could be easily adapted to specific requirements of a sample. One point that might require further investigation is that in the PMRs, the sample gets relatively close to the metallic walls, whose susceptibility may cause static magnetic field distortions.[27]

ACKNOWLEDGMENTS

The authors thank Dr. R. Stonies and Professor E. Voges from the High Frequency Institute, Technical University of Dortmund, for expert technical assistance. This work was supported by the DFG (Project No. SU 192/18-1).

[1] H. Mahdjour, W. G. Clark, and K. Baberschke, Rev. Sci. Instrum. **57**, 1100 (1986).
[2] Y. Morita and K. Ohno, J. Magn. Reson., Ser. A **102**, 344 (1993).
[3] H. J. Mamin, R. Budakian, and D. Rugar, Rev. Sci. Instrum. **74**, 2749 (2003).
[4] G. Boero, M. Bouterfas, C. Massin, F. Vincent, P.-A. Besse, R. S. Popovic, and A. Schweiger, Rev. Sci. Instrum. **74**, 4794 (2003).
[5] R. Narkowicz, D. Suter, and R. Stonies, J. Magn. Reson. **175**, 275 (2005).
[6] T. Obata, M. Pioro-Ladrière, T. Kubo, K. Yoshida, Y. Tokura, and S. Tarucha, Rev. Sci. Instrum. **78**, 104704 (2007).
[7] W. Froncisz, T. Oles, and J. S. Hyde, Rev. Sci. Instrum. **57**, 1095 (1986).
[8] B. Simovič, P. Studerus, S. Gustavsson, R. Leturcq, K. Ensslin, R. Schuhmann, J. Forrer, and A. Schweiger, Rev. Sci. Instrum. **77**, 064702 (2006).
[9] J. W. Sidabras, R. R. Mett, W. Froncisz, T. G. Camenisch, J. R. Anderson, and J. S. Hyde, Rev. Sci. Instrum. **78**, 034701 (2007).
[10] D. Rugar, R. Budakian, H. J. Mamin, and B. W. Chui, Nature (London) **430**, 329 (2004).
[11] I. Popa, T. Gaebel, M. Domhan, C. Wittmann, F. Jelezko, and J. Wrachtrup, Phys. Rev. B **70**, 201203(R) (2004).
[12] F. H. L. Koppens, C. Buizert, K. J. Tielrooij, I. T. Vink, K. C. Nowack, T. Meunier, L. P. Kouwenhoven, and L. M. K. Vandersypen, Nature (London) **442**, 766 (2006).
[13] T. L. Peck, R. L. Magin, and P. C. Lauterbur, J. Magn. Reson., Ser. B **108**, 114 (1995).
[14] Y. Maguire, I. L. Chuang, S. Zhang, and N. Gershenfeld, Proc. Natl. Acad. Sci. U.S.A. **104**, 9198 (2007).
[15] IEC 60169–15, 1979.
[16] D. I. Hoult and R. E. Richards, J. Magn. Reson. **24**, 71 (1976).
[17] E. Pettenpaul, H. Kapusta, A. Weisgerber, H. Mampe, J. Luginsland, and I. Wolff, IEEE Trans. Microwave Theory Tech. **36**, 294 (1988).
[18] J. S. Hyde, W. Froncisz, and T. Oles, J. Magn. Reson. **82**, 223 (1989).
[19] The simple estimate for the cavity resonator $\Lambda=B_1^r/\sqrt{P_{\mu w}}=\sqrt{\mu_0 Q/2\pi f_{\mu w} V_c}$ gives a value of 0.07 mT/W$^{1/2}$ for the cavity with the quality factor $Q=1000$ at the frequency $f_{\mu w}=14$ GHz.
[20] R. Stonies, "Hybrid compact circulators in the thin-film technology," Ph.D. thesis, Technical University of Dortmund, 2007.
[21] M. Jaworski, A. Sienkiewicz, and Ch. P. Scholes, J. Magn. Reson. **124**, 87 (1997).
[22] D. I. Hoult, Prog. Nucl. Magn. Reson. Spectrosc. **12**, 41 (1978).
[23] J. A. Weil, J. R. Bolton, and J. E. Wertz, *Electron Paramagnetic Resonance* (Wiley, New York, 1994).
[24] H. Wahlquist, J. Chem. Phys. **35**, 1708 (1961).
[25] S. Linden, Ch. Enkirch, M. Wegener, J. Zhou, T. Koschny, and C. M. Soukoulis, Science **306**, 1351 (2004).
[26] K. Ehrmann, M. Gersbach, P. Pascoal, F. Vincent, C. Massin, D. Stamou, P.-A. Besse, H. Vogel, and R. S. Popovic, J. Magn. Reson. **178**, 96 (2006).
[27] A. G. Webb and S. C. Grant, J. Magn. Reson., Ser. B **113**, 83 (1996).